J. Fluid Mech. (2002), *vol.* 456, *pp.* 161–182.
DOI: 10.1017/S0022112001007510 Printed in the United Kingdom

The effects of thermal modulation upon the onset of Marangoni–Bénard convection

By A. C. OR AND R. E. KELLY

Department of Mechanical and Aerospace Engineering,
University of California, Los Angeles, CA 90095-1597, USA

(Received 11 November 2000 and in revised form 25 September 2001)

The effects of thermal modulation with time on the thermocapillary instability of a thin horizontal fluid layer with a deformable free surface are investigated on the basis of linear stability theory. First, a sinusoidal heating with a mean component is applied at the lower wall, corresponding to boundary conditions either in the form of prescribed temperature or heat flux. For finite-wavelength convection the thermal modulation exerts a strong effect, giving rise to a family of looped regions of instability corresponding to alternating synchronous or subharmonic responses. In the case of prescribed heat flux, the critical curve consists of significantly fewer loops than in the case of prescribed temperature. Thermal modulation with moderate modulation amplitude tends to stabilize the mean basic state, and optimal values of frequency and amplitude of modulation are determined to yield maximum stabilization. However, large-amplitude modulation can be destabilizing. A basic state with zero mean is then considered and the critical Marangoni number is obtained as a function of frequency. The effects of modulation are also investigated in the long-wavelength limit. For the case of prescribed temperature, the modulation does not affect the onset of the long-wavelength mode associated with the mean basic state and a purely oscillating basic state is always stable with respect to long-wavelength disturbances. For the case of prescribed heat flux both at the wall and free surface, by contrast, thermal modulation exerts a significant effect on the onset of convection from a mean basic state and long-wavelength convection can occur even for a purely oscillating basic state. The modulation can be stabilizing or destabilizing, depending on the frequency.

1. Introduction

The problem of how an oscillatory, non-planar shear can affect the onset of Marangoni–Bénard (MB) convection has been investigated on a linear basis (Or & Kelly 1995, 1998). It was then concluded that such unsteady shear can be used to stabilize significantly both the long-wavelength mode (Scriven & Sternling 1964) that tends to be dominant in a microgravity environment and the finite-wavelength mode that tends to be dominant on earth (Pearson 1958). For the long-wavelength mode, however, the result is sensitive to the choice of modulating frequency, and significant destabilization can occur over certain bands of frequency.

In order to provide a contrast to the use of unsteady shear, the possibility of thermal modulation for stabilization is considered here. Thermal modulation can be easier to implement than shear. The effects of thermal modulation on the onset of Rayleigh–Bénard (RB) convection have been studied quite extensively (see, for instance, Yih & Li 1972; Davis 1976; Niemela & Donnelly 1986; Swift & Hohenberg 1987;

Donnelly 1990; Or & Kelly 1999). By contrast, similar investigations for modulated MB convection are significantly fewer. Gershuni, Nepomnyashchy & Velarde (1992) considered thermal modulation when a purely oscillatory heat flux is applied on the non-deformable free surface of a fluid which is infinitely deep. They predicted a critical Marangoni number that decreases as the Prandtl number increases. The critical Marangoni number occurred for a subharmonic mode, just as is predicted here in § 3.1 for high-frequency modulated heating from below. We have presented some preliminary results concerning the effects of temperature modulation from below on the onset of finite-wavelength disturbances when the heating has a non-zero mean (Kelly & Or 1998). The present study will consider more general modulation and include basic states with zero mean as well as non-zero mean temperature gradients. While this paper was being revised, the results of Skarda (2001) concerning the effects of gravity modulation on MB convection were published, and comparison of his results with our own for thermal modulation will be made when appropriate.

We consider MB convection in a layer of fluid with a surface tension dependent upon temperature subjected to a thermal modulation applied only at the lower wall, either as a prescribed temperature or a prescribed heat flux. In either case, the modulation is assumed to be sinusoidal in time and is applied uniformly along the wall. The two cases with prescribed temperature or heat flux can be considered as two limits of more realistic thermal boundary conditions occurring in laboratory experiments. The fluid is bounded above by a deformable free surface.

The model used here is a single-layer model with a thermal boundary condition at the free surface depending on a constant Biot number. For laboratory experiments, however, usually a two-layer (gas–liquid) configuration with finite depths has been used. It is therefore important to argue that a single-layer approximation is adequate for the two-layer configuration. For the steady basic-state problem, various investigators (Golovin, Nepomnyashchy & Pismen 1995; Pérez-García, Echebarria & Bestehorn 1998; Regnier, Dauby & Lebon 2000) have shown that by allowing the Biot number to be a function of the material property ratios of the two layers and assuming the gas to have negligible mass, the one-layer stability results match the two-layer results very well. However, when the basic state is time-varying, as in the present case, the Biot number is in general a complex parameter which depends also on the modulating frequency. If the depths of the two layers are comparable, then the non-dimensional frequency of the air layer will be much less than that of the liquid layer because the diffusivity of air is much larger than that of liquids. This disparity means that the air layer will be quasi-steady for moderate frequencies and so the temperature and temperature gradient will be in phase, i.e. the Biot number will be nearly real and independent of frequency. This result will hold even more for the case of a thin layer of air. The one-layer model should then be a good approximation. The expressions for the complex Biot number in terms of material and modulation parameters are derived in Appendix B.

Because subcritical convection is associated with steady thermocapillary convection and can also be associated with the effects of oscillation, the present results must be complemented by a weakly nonlinear analysis. In order to do such an analysis, the critical values of the Marangoni number must be established first as a function of the various parameters, which is our aim here. Our study will focus mainly on the determination of the critical curves as functions of both modulation amplitude and frequency, as well as the physical parameters corresponding to the fluid layer. The two modes found here are the synchronous (S) mode, with the same period as the modulation, and the subharmonic (H) mode, with twice the period of the modulation.

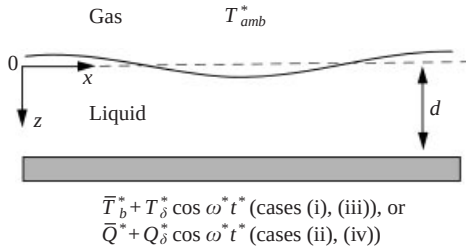

FIGURE 1. Geometric configuration.

The analysis of the finite-wavelength modes of convection yields some new results which will be considered in detail and compared to those occurring for RB convection. The effects of modulation on the onset condition of long-wavelength disturbances will also be addressed. For the case of zero mean temperature, the long-wavelength limit is found to predict instability at a finite Marangoni number only in the case of prescribed heat flux. This appears to be a new result which resembles to some degree the long-wavelength instability due to shear.

The mathematical formulation will be presented in § 2, followed by the analysis and results in § 3. In § 4, we provide some concluding remarks.

2. Mathematical formulation

2.1. *The basic state*

Consider an infinite horizontal layer of a Boussinesq liquid with a mean thickness d, bounded below by a non-slip wall and above by a deformable free surface. Refer to figure 1. The layer of liquid is cooled from above and heated from below. For the time-averaged state, the upper surface is governed by a mixed heat transfer condition and the lower wall is prescribed at a constant temperature $\bar{T}^*_b$ or constant heat flux $\bar{Q}^*$ (asterisk denotes dimensional variables). For long-wavelength disturbances, the heat flux will be prescribed at both the wall and the free surface. In addition to the mean field, a thermal modulation is applied at the lower wall only, again either as a prescribed temperature $T^*_\delta \cos \omega^* t^*$ or heat flux $Q^*_\delta \cos \omega^* t^*$, where T^*_δ and Q^*_δ are the amplitudes of the modulating temperature and heat flux, respectively, and ω^* is the modulating frequency. The fluid layer is considered sufficiently thin that the buoyancy force is negligible for the frequency range investigated. Further justification of this assumption will be given at the end of § 2.2.

The basic state is conductive and no fluid motion occurs, unlike the case of shear-modulated flow (Or & Kelly 1995, 1998). The basic temperature, T^*, can be expressed through a non-dimensional temperature T, defined by

$$T^*(z,t) = T^*_0 + \Delta T^* T(z,t), \tag{1}$$

where T^*_0 and ΔT^* are appropriate temperature scales to be introduced for the various situations to be considered, $z = z^*/d$ extends into the layer from the free surface, and $t = \omega^* t^*$. For convenience we decompose T^* and T so that $T^* - T^*_0 = \bar{T}^* + \tilde{T}^*$ and $T = \bar{T} + \tilde{T}$, where the first component is time-independent, i.e. the mean component. The second component is purely oscillatory.

We consider four different cases with modulation according to different prescribed thermal conditions at the lower wall. These are: (i) prescribed temperature with non-zero time mean; (ii) prescribed heat flux with non-zero mean; (iii) prescribed

temperature with zero-mean; and (iv) prescribed heat flux with zero-mean. For cases (i)–(ii), the mean basic state can be expressed as

$$\bar{T}(z) = z, \tag{2}$$

For cases (iii)–(iv), the mean basic state is isothermal, or simply $\bar{T}(z) = 0$.

For the dimensional quantities, the following scalings are appropriate for cases (i)–(iv), respectively,

$$\text{(i)}: \quad T_0^* = \bar{T}_s^*, \quad \Delta T^* = (\bar{T}_b^* - \bar{T}_s^*) = Bi(\bar{T}_s^* - T_{amb}^*), \tag{3a}$$

$$\text{(ii)}: \quad T_0^* = \bar{T}_s^*, \quad \Delta T^* = \bar{Q}^* d/K = Bi(\bar{T}_s^* - T_{amb}^*), \tag{3b}$$

$$\text{(iii)}: \quad T_0^* = \bar{T}_s^* = \bar{T}_b^* = T_{amb}^*, \quad \Delta T^* = T_\delta^*, \tag{3c}$$

$$\text{(iv)}: \quad T_0^* = \bar{T}_s^* = \bar{T}_b^* = T_{amb}^*, \quad \Delta T^* = Q_\delta^* d/K. \tag{3d}$$

In equations (3*a*) and (3*b*), Bi represents the Biot number, assumed to be real and independent of frequency ($Bi = hd/K$, K denoting thermal conductivity and h being a heat transfer coefficient; see Appendix B for a more general formulation). In the equations, subscripts b and s denote the bottom wall and the free surface, respectively.

The fluctuating temperature $\tilde{T}(z,t)$ is governed by the equation

$$2\omega \tilde{T}_t = \tilde{T}_{zz}, \tag{4}$$

where $\omega = \omega^* d^2/2\kappa$ is the non-dimensional frequency and κ is the fluid thermal diffusivity.

On the free surface ($z = 0$), we use the mixed boundary condition

$$\tilde{T}_z(0,t) = Bi\tilde{T}(0,t), \tag{5}$$

for all cases. The thermal condition at the lower-wall ($z = 1$) for the four cases (i)–(iv) are

$$\text{(i)}: \quad \tilde{T}(1,t) = \epsilon_T \cos t, \tag{6a}$$

$$\text{(ii)}: \quad \tilde{T}_z(1,t) = \epsilon_F \cos t, \tag{6b}$$

$$\text{(iii)}: \quad \tilde{T}(1,t) = \cos t, \tag{6c}$$

$$\text{(iv)}: \quad \tilde{T}_z(1,t) = \cos t. \tag{6d}$$

For cases (i) and (ii), ϵ_T and ϵ_F are, respectively, defined by $\epsilon_T = T_\delta^*/\Delta T^*$ and $\epsilon_F = Q_\delta^*/\bar{Q}^*$. Using the diffusion equation and the above boundary conditions, we determine the oscillating component of temperature for cases (i) and (ii) to be, respectively,

$$\text{(i)}: \quad \tilde{T}(z,t) = \frac{\epsilon_T}{2}\left\{\frac{\sqrt{\mathrm{i}2\omega}\cosh\sqrt{\mathrm{i}2\omega}\,z + Bi\sinh\sqrt{\mathrm{i}2\omega}\,z}{\sqrt{\mathrm{i}2\omega}\cosh\sqrt{\mathrm{i}2\omega} + Bi\sinh\sqrt{\mathrm{i}2\omega}}\mathrm{e}^{\mathrm{i}t} + \text{c.c.}\right\}, \tag{7a}$$

$$\text{(ii)}: \quad \tilde{T}(z,t) = \frac{\epsilon_F}{2}\left\{\frac{\sqrt{\mathrm{i}2\omega}\cosh\sqrt{\mathrm{i}2\omega}\,z + Bi\sinh\sqrt{\mathrm{i}2\omega}\,z}{\mathrm{i}2\omega\sinh\sqrt{\mathrm{i}2\omega} + Bi\sqrt{\mathrm{i}2\omega}\cosh\sqrt{\mathrm{i}2\omega}}\mathrm{e}^{\mathrm{i}t} + \text{c.c.}\right\}, \tag{7b}$$

where 'c.c.' denotes the complex conjugate. If we set $\epsilon_T = \epsilon_F = 1$, equations 7(*a*) and 7(*b*) represent the oscillatory basic state for cases (iii) and (iv), respectively. Thus, when expressed in real form, we have for cases (i) and (ii), respectively,

$$\text{(i)}: \quad T(z,t) = z + \tfrac{1}{2}\epsilon_T(\phi_{tc}(z)\cos t + \phi_{ts}(z)\sin t), \tag{7c}$$

$$\text{(ii)}: \quad T(z,t) = z + \tfrac{1}{2}\epsilon_F(\phi_{fc}(z)\cos t + \phi_{fs}(z)\sin t), \tag{7d}$$

and we have for case (iii) and (iv), respectively,

$$\text{(iii)}: \quad T(z,t) = \tfrac{1}{2}(\phi_{tc}(z)\cos t + \phi_{ts}(z)\sin t), \tag{7e}$$

$$\text{(iv)}: \quad T(z,t) = \tfrac{1}{2}(\phi_{fc}(z)\cos t + \phi_{fs}(z)\sin t), \tag{7f}$$

where the functions ϕ_{tc}, ϕ_{ts}, ϕ_{fc} and ϕ_{fs} are left implicit here but can be readily determined from equations 7(a) and 7(b).

2.2. *The stability problem*

To investigate the stability of the basic state, let $(T^* - T_0^*)/\Delta T^* = T(z,t) + \theta(x,y,z,t)$ and allow the fluid velocity to be non-zero, scaled according to $\boldsymbol{u}^* = (\kappa/d)\boldsymbol{u}(x,y,z,t)$. Following Or & Kelly (1998), we obtain the linearized perturbation equations,

$$2\omega Pr^{-1}\nabla^2 w_t - \nabla^4 w = 0, \tag{8}$$

$$2\omega\theta_t - \nabla^2\theta = -T_z(z,t)\,w, \tag{9}$$

where w is the vertical component of velocity and θ is the perturbation temperature. The lower wall is non-permeable and non-slip, according to the two conditions

$$w(x,y,1,t) = w_z(x,y,1,t) = 0. \tag{10}$$

The thermal condition there for cases (i) and (iii) is

$$\theta(x,y,1,t) = 0. \tag{11}$$

On the other hand, the thermal condition for cases (ii) and (iv) is

$$\theta_z(x,y,1,t) = 0. \tag{12}$$

The perturbation boundary conditions at the deformed free surface are evaluated at the mean height $z = 0$. These linearized conditions consist of equations for the normal and the tangential stress balances, the free surface heat condition and a kinematic relationship. They are, respectively,

$$2\omega Pr^{-1}w_{zt} - w_{zzz} - 3\nabla_\perp^2 w_z + \frac{1}{Cr}(B - \nabla_\perp^2)\nabla_\perp^2\eta = 0, \tag{13}$$

$$\nabla_\perp^2 w - w_{zz} = M\nabla_\perp^2(T_z\eta + \theta), \tag{14}$$

$$(T_{zz}\eta + \theta_z) = Bi(T_z\eta + \theta), \tag{15}$$

$$2\omega\eta_t = w, \tag{16}$$

where $\nabla_\perp^2 = (\partial_{xx} + \partial_{yy})$. The non-dimensional parameters are: Prandtl number $Pr = \nu/\kappa$, crispation number $Cr = \rho\nu\kappa/\sigma_0 d$ where σ_0 is the reference surface tension, Bond number $B = \rho g d^2/\sigma_0$ where g is acceleration due to gravity, and Marangoni number $M = \gamma\Delta T^* d/\rho\nu\kappa$ where $\gamma = -(\mathrm{d}\sigma/\mathrm{d}T^*)|_{T_0^*}$. We seek solutions with the following representation,

$$(w,\theta,\eta) = (W(z,t), \Theta(z,t), N(t))\exp(\mathrm{i}(k_x x + k_y y)) + \text{c.c.} \tag{17}$$

The horizontally decomposed system depends on z, t and k, where $k^2 = (k_x^2 + k_y^2)$.

In the analysis of Skarda (2001), $T_z = 1$ and a time-varying buoyancy term is included in equation (8). However, only a non-deformable surface was considered and so neither B nor Cr entered into his problem. An isothermal wall condition was imposed at $z = 1$.

3. Analysis and results

We make a couple of preliminary remarks which help to put the results in proper perspective. First, B/Cr measures in part the deformation effect of the disturbed free surface. This parameter distinguishes between earthbound and microgravity conditions and is important usually only for the long-wavelength mode of convection. However, it should be pointed out that without gravity a flat-layer geometry can only be realized by pinning the free surface at the sidewall and properly filling the container (see e.g. Kamotani 1997). Therefore, an infinite flat-layer assumption may not be an accurate description of a specific experiment in space. Secondly, for the range of very high modulating frequency, buoyancy can become important for instability of the thermal Stokes layer on earth. The onset of this instability was estimated to be $Ra_c \approx 6.6 \times 10^4$ for $Pr > 2$ (Or & Kelly 1999). For a thin layer, however, such a value of Ra is considered unrealistically high. For the range of parameters considered, neglect of the buoyancy force appears to be well justified.

3.1. *Finite wavelength convection*

We begin by considering the effects of modulation on the stability of finite-wavelength disturbances, which is studied here numerically. Later, we will give a brief account of the stability problem in the long-wavelength limit for varous cases.

The dependent variables $W(z,t)$ and $\Theta(z,t)$ are expanded in terms of the Chebyshev functions $T_n(z)$, as follows:

$$W(z,t) = \sum_{0}^{N_t} W_n(t) T_n(z), \quad \Theta(z,t) = \sum_{0}^{N_t} \Theta_n(t) T_n(z), \tag{18}$$

where N_t is a truncation parameter, and W_n and Θ_n are the Chebyshev coefficients. Through a numerical procedure described in Or (1997), we reduce the system to an infinite set of ordinary differential equations for the Chebyshev coefficients. These coefficients are functions of time only and are truncated and arranged in a vector form $\boldsymbol{X}(t)$. The boundary conditions are incorporated by use of the tau method. We seek solutions in Floquet form, in which $\boldsymbol{X}(t)$ can be expanded as follows:

$$\boldsymbol{X}(t) = \sum_{n=-N_p}^{N_p} \boldsymbol{X}_n \, \mathrm{e}^{\mathrm{i}nt+\sigma t}, \tag{19}$$

where σ denotes the complex Floquet exponent and N_p is a second truncation parameter. The expansion of each dependent variable takes N_t Chebyshev functions in z and $2N_p + 1$ sinusoidal functions in time.

The numerical procedure we used to compute the neutral curves for the stability problem is of an iterative type. The procedure was documented in detail in Appendix A of Or (1997). The Chebyshev coefficients are functions of time and when arranged in a vector form they satisfy a matrix equation with entries which are periodic functions of time. When expanded in a Fourier Floquet series, the matrix equation yields an infinite sequence of matrix equations with time-independent coefficients. The sequence of equations is solved by successive elimination based on a Newton–Raphson method. We have a choice of iterating for either synchronous or subharmonic solutions to obtain a neutral Marangoni number from the real matrix equations, or for a given M we can iterate for the growth rate and the Floquet exponent from the complex matrix equations. The solution obtained depends crucially on the initial guess. Since a set of parameters can yield multiple values of M, there is always a possibility that

the neutral value of M obtained does not correspond to the lowest curve. For cases (i) and (ii), the unmodulated solution is known *a priori* and can be used as a basis for computing solutions as the modulating amplitude increases. For cases (iii) and (iv), the lowest neutral curve is obtained after performing a large number of iterations based on a wide range of initial guesses, many of which start from values of M that are orders of magnitude smaller than the final value, in order to guarantee that neutral solutions with a lower M value do not exist. Most of the solutions computed here use 32 Fourier modes and 20 Chebyshev modes. The convergence criterion used is that, by increasing the number of Fourier and Chebyshev modes each by 4, the value of M changes only within 1%. Most of our solutions are obtained for $\omega \approx 1$ or greater. The convergence properties for these solutions are reasonably good. Typically, it takes 4–8 iterations to converge. Poor convergence is typically encountered for smaller values of frequency, and so we do not present results for the low-frequency regime, which can be investigated best by the use of another approach (e.g. WKB; see Or 2001).

The nominal values for the parameters for the numerical study are $Pr = 7$, $B = 0.15$ and $Cr = 2 \times 10^{-6}$ which are values typical of an experiment done on earth. We also let $Bi = 0.1$ unless otherwise stated. For the unmodulated problem, the Pearson mode (Pearson 1958) is the mode that occurs at a finite wavenumber. This is the critical mode with these parameters.

Case (i). *Temperature modulation,* $\bar{T} \neq 0$

We consider the stability limit of the basic state for a range of ϵ_T. In figure 2(a), we show the critical curve at $\omega = 1$. For this value of ω, the modulating and thermal diffusive time scales are comparable in magnitude. This curve has many branches, consisting of alternate pairs of S modes (solid) and H modes (dashed) beyond $\epsilon_T \approx 2.6$. The character of the critical curve is similar to that of modulated RB convection first obtained by Yih & Li (1972). For our parameters, unmodulated MB convection has $M_{c0} \approx 83.4$, corresponding to $k_{c0} \approx 2.03$. As ϵ_T increases from zero, M_c increases to a maximum of about 115 near $\epsilon_T = 4$. Then, M_c decreases as ϵ_T continues to increase. When the modulating amplitude exceeds $\epsilon_T \approx 14.3$, M_c drops below M_{c0} so that destabilization occurs. Skarda (2001) shows detailed results in his figures 5–7 in terms of amplitude of modulation versus the inverse of the frequency for different M. A qualitatively similar picture emerges for fixed frequency, namely, a region of synchronous instability for low-amplitude modulation followed by a region of stability that is terminated by a synchronous or subharmonic instability for larger amplitudes. The nesting of branches is densest near the maximum value of M_c. In figure 2(b), we show the critical wavenumber curves. The critical wavenumber is discontinuous between adjacent branches of the critical curve. Again, a similar character is observed for modulated RB convection (see Yih & Li 1972).

We consider now the stability limit for a range of ω, with ϵ_T prescribed at a fixed value; see figures 3(a) and 3(b). Two values of amplitude are considered: $\epsilon_T = 3$ and $\epsilon_T = 5$. As ϵ_T increases, more branches of S and H modes appear. The nesting seems to be denser at low values of ω. The portion of the curve below $\omega = 1$ is excluded because of a decrease in numerical accuracy. For large ω, we observe that M_c tends to the unmodulated value. For $\omega^{1/2} \gg 1$, the thermal modulation can only affect the thermal Stokes layer, which is close to the lower wall and of thickness $O(\omega^{-1/2})$. The oscillatory thermal field becomes increasingly unimportant in affecting the free surface. Therefore, for $\omega^{1/2} \gg 1$, the instability is driven by the mean temperature gradient. The disturbances respond to the modulation in synchronous fashion. A similar behaviour occurs in modulated RB convection for the same values of ϵ_T,

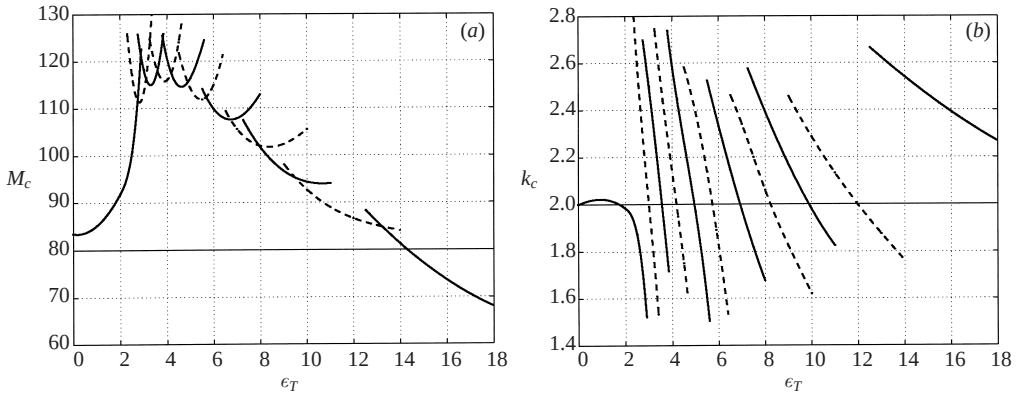

FIGURE 2. (*a*) Critical curve M_c of the modulated Pearson mode of case (i) at $\omega = 1$ for a range of modulating amplitude ϵ_T: synchronous solution (solid) and subharmonic (dashed). (*b*) The corresponding k_c.

where $Ra_c \to Ra_{c0}$ when $\omega^{1/2}$ is greater than 5. Skarda (2001) also finds that M_c tends to the unmodulated value for very large ω, although for a different reason.

A pronounced local maximum in stabilization occurs near $\omega^{1/2} = 3$ in figure 3(*a*) and near $\omega^{1/2} \approx 4$ in figure 3(*b*). The maxima in figures 3(*a*) and 3(*b*) shift towards higher frequencies and have a larger value as ϵ_T increases, although this trend cannot continue indefinitely. Hence, an optimal combination of ϵ_T and ω would seem to exist. The maximum marks the transition between the two types of balance occurring at low and high frequencies. For lower or moderate frequency, both mean and oscillatory components of temperature gradient are important for the unstable mode. For higher modulating frequency, the oscillatory component becomes unimportant. In figures 3(*c*) and 3(*d*), we show the curves of the critical wavenumber, corresponding to M_c in figures 3(*a*) and 3(*b*), respectively. Again, these curves are discontinuous. It is not clear from the results of Yih & Li (1972) whether a similar behaviour with ω exists for modulated RB convection because they stopped their calculations at a frequency for which the maximum stabilization is still increasing. However, it is likely to occur also for RB convection.

One significant difference between our results for thermal modulation and Skarda's results for gravity modulation is that Skarda (2001) has found that the subharmonic instability can occur in a closed region, at least for $Pr \approx 1$. We have not considered such a low value of Pr and have found only nested regions, as shown in figures 2 and 3.

Case (ii). *Heat-flux modulation,* $\bar{T} \neq 0$

For $Bi = 0.1$, the unmodulated critical point occurs at $k_c \approx 1.05$ and $M_c \approx 58.18$. Again, we first consider a prescribed frequency at $\omega = 1$ and show the variation of M_c and k_c for a range of ϵ_F. Similar to the results of figure 2(*a*), figure 4(*a*) shows a critical curve corresponding to an S mode as ϵ_F increases from zero. Again, the modulation is initially stabilizing. However, unlike case (i), even for moderately large values of ϵ_F up to 30, we have found only two branches of the critical curve: the first one corresponds to an S mode, followed by another branch corresponding to an H mode. The two branches intersect near $\epsilon_F = 13.5$, at which value maximum stabilization occurs. Despite this larger value of ϵ_F for case (ii), the maximum degree of stabilization for the two cases (i) and (ii) are comparable, about $1.4M_{c0}$. In figure 4(*b*),

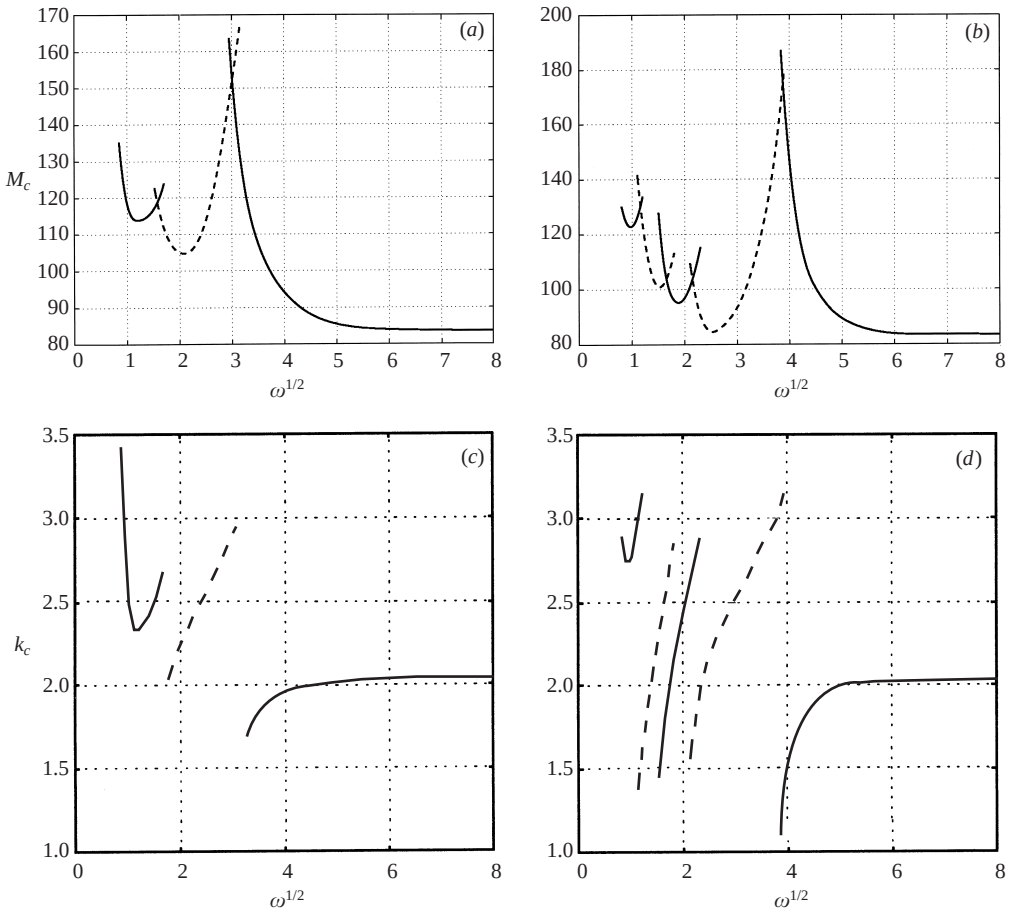

FIGURE 3. Critical curve M_c of the modulated Pearson mode of case (i) versus $\omega^{1/2}$, at (*a*) $\epsilon_T = 3$ and (*b*) $\epsilon_T = 5$, showing the stability limit for a range of modulating frequency: synchronous solution (solid) and subharmonic (dashed) line. The corresponding curves for k_c are shown in (*c*) and (*d*), respectively.

we show the corresponding curves for k_c. Unlike the critical wavenumber of case (i), here the critical wavenumber for the subharmonic branch stays fairly constant at $k_c \approx 2$. For the synchronous branch, k_c varies between 0.5 and 1.1.

Next, we consider the critical values for a range of $\omega^{1/2}$, with ϵ_F prescribed at a fixed value. For more dramatic results, we consider larger values for ϵ_F than for ϵ_T in case (i). In figure 5, the critical curves shown are obtained at $\epsilon_F = 5$ (thin line) and $\epsilon_F = 15$ (heavy lines). For $\epsilon_F = 5$, figure 5(*a*) shows only a single branch of the critical curve (thin line) corresponding to an S mode, quite unlike the behaviour shown in figure 3(*b*). For $\epsilon_F = 15$, we obtain two branches (heavy lines). Now a subharmonic mode precedes a synchronous mode in the range of ω shown. Again, we will not consider any critical point below $\omega = 1$ for numerical reasons. Comparing figure 5(*a*) to figure 3(*b*), we observe that M_c again tends to a constant value for large ω, as has been explained in the earlier discussion of figure 3(*b*). The values at transition to a constant M_c for the two cases are about the same, at $\omega^{1/2} = 5$, but the value of $\omega^{1/2}$ for maximum stabilization is lower for case (ii) than for case (i). In figure 5(*b*), we show the corresponding k_c for the curves.

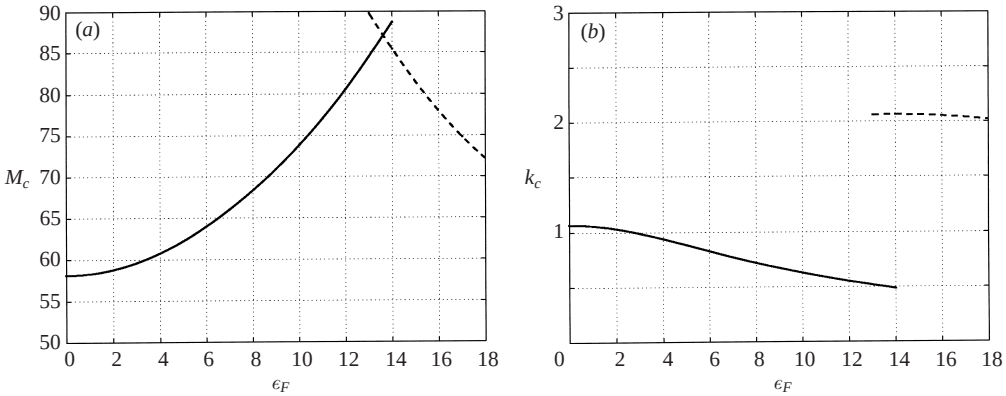

FIGURE 4. Critical curves of case (ii) computed at $\omega = 1$ for a range of modulating amplitude ϵ_F. (a) M_c and (b) the corresponding k_c.

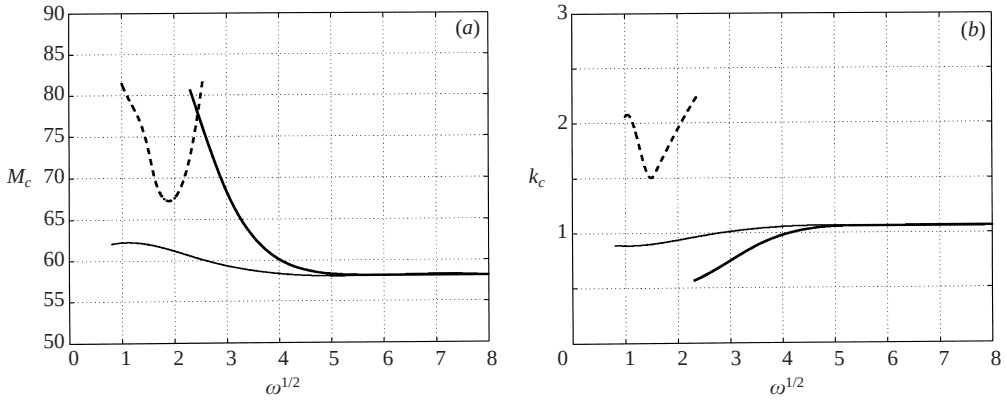

FIGURE 5. (a) Critical curves of case (ii) showing M_c versus $\omega^{1/2}$ for $\epsilon_T = 5$ (thin line) and for $\epsilon_T = 15$ (heavy lines): synchronous solution (solid) and subharmonic (dashed). (b) The corresponding curves of k_c.

The family of branches of the critical curve for case (ii) is therefore significantly different from that of case (i); many more branches of curves for the alternating S and H modes occur in case (i). Corresponding results for modulated RB convection with case (ii) conditions do not seem to exist and so no comparison can be made in this respect.

Case (iii). *Temperature modulation,* $\bar{T} = 0$

When modulated by a purely sinusoidal temperature or heat flux with sufficiently large amplitude, a liquid layer can become unstable and give rise to convection. This situation has been considered for buoyancy-driven convection by Or & Kelly (1999); see also the references listed therein. When the basic state has no mean temperature difference, the Rayleigh number is defined on the basis of the modulating amplitude. At sufficiently high frequency, the instability of this thermal Stokes layer has a self-similar thickness scale, where Ra_c and k_c scale according to $\omega^{3/2}$ and $\omega^{1/2}$, respectively. The thickness of the thermal Stokes layer varies as $\omega^{-1/2}$.

Alternating bands of synchronous and subharmonic instability again occur. For $k \sim O(1)$, these bands terminate in loop-shaped regions. In figure 6(a), with $\omega^{11/2} = 2$,

we show a few of these loop-shaped regions as a function of wavenumber. Each loop has a minimum in M at which the unstable region terminates. There is a global minimum, corresponding to $M_c = 1135$ and $k_c = 2.2$. Figure 6(b) shows the critical curve for a range of $\omega^{1/2}$. Like the case of modulated RB convection (Or & Kelly 1999), the critical curve consists of multiple alternating pairs of loops due to the S mode (solid lines) and H mode (dashed lines). Note that M_c is greater than 10 times the value of M_{c0} for steady heating. We note from the definitions of Marangoni number that the M for case (iii) is equal to the M for case (i) multiplied by ϵ_T, defined as the ratio $T^*_\delta/(\bar{T}^*_b - \bar{T}^*_s)$. For case (iii), this ratio tends to infinity. In order for convection to occur in the case of a zero-mean basic state, we require $M_c \to 0$ as $\epsilon_T \to \infty$. The results of figure 2(a) certainly show the trend that M_c continues to decrease as ϵ_T increases. In figure 6(b), the loops become increasingly small and closely packed as ω decreases towards zero. This situation is similar to that predicted for Faraday instability of a free surface in a viscous fluid (Kumar 1996; Cerda & Tirapegui 1997); see also figure 3(b). The first loop (from right to left) is subharmonic. No additional loop to the right-hand side of this loop could be found. The right-hand side of this loop diverges significantly faster than $\omega^{1/2}$. It suggests that there is no self-similar scale for the critical point. This result is not surprising since thermocapillarity is concentrated near the upper surface, unlike RB convection. For MB convection modulated from below, the destabilizing force involving the surface temperature becomes detached from the thermal Stokes layer at the lower wall at high frequency. This difference with modulated RB convection is important to note. In figure 6(c), we show the corresponding critical curve for k_c, which qualitatively resembles the branches of k_c obtained for RB convection (Or & Kelly 1999). The rightmost branch shows that k_c increases significantly slower than $O(\omega^{-1/2})$, again consistent with the fact that there is no self-similar scale in the thermal Stokes layer.

Case (iv). *Heat-flux modulation,* $\bar{T} = 0$

It is of interest first to see how M depends on k. In figure 7, we show the neutral curves of $M(k)$ for two modulating frequencies: $\omega^{1/2} = 2$ (thin curve) and $\omega^{1/2} = 3.5$ (thick curves). For $\omega^{1/2} = 2$, the neutral curve consists of only one loop of the subharmonic mode, with a critical point at $k_c \approx 2.0$ and $M_c \approx 2215$. There seems to be no branch of the neutral curve corresponding to long-wavelength convection. For $\omega^{1/2} = 3.5$, the subharmonic loop is critical at $k_c \approx 2.2$ and $M_c \approx 3615$. In addition, now there is a synchronous branch (solid curve) with a minimum at $k = 0$. For $k = 10^{-4}$, $M \approx 2.43 \times 10^4$. These particular results correspond to $Bi = 0$, chosen so comparison can be made later to the results of § 3.2. The finite-k loops (dashed curves) are not sensitive to Bi. For instance, at $Bi = 0.1$ and $\omega^{1/2} = 2$, M_c increases only by 3.4%.

In figure 8, we track the critical point of the finite-k mode for a range of $\omega^{1/2}$. There is a dramatic difference between this critical curve and that of case (iii) shown in figure 6(b). In the range of figure 8(a), the critical curve consists of only two branches. Moreover, this critical curve does not involve an alternate pair of S and H modes, as occurring in all other situations. Here, both branches correspond to subharmonic modes. In figure 8(b), we show the corresponding critical curve for k_c.

The occurrence of two adjacent subharmonic branches is due to a double minima in the neutral curve $M(k)$. Consider $\omega^{1/2} = 2.3$, which is very close to the value where a double minima occurs. Here, $M_c \approx 2708$ with a critical wavenumber $k_c \approx 2.2$. A second local minimum occurs at $k \approx 1.4$ with slightly higher M (to within 1% of M_c). As ω increases, the mode with the larger scale becomes critical, but its k_c

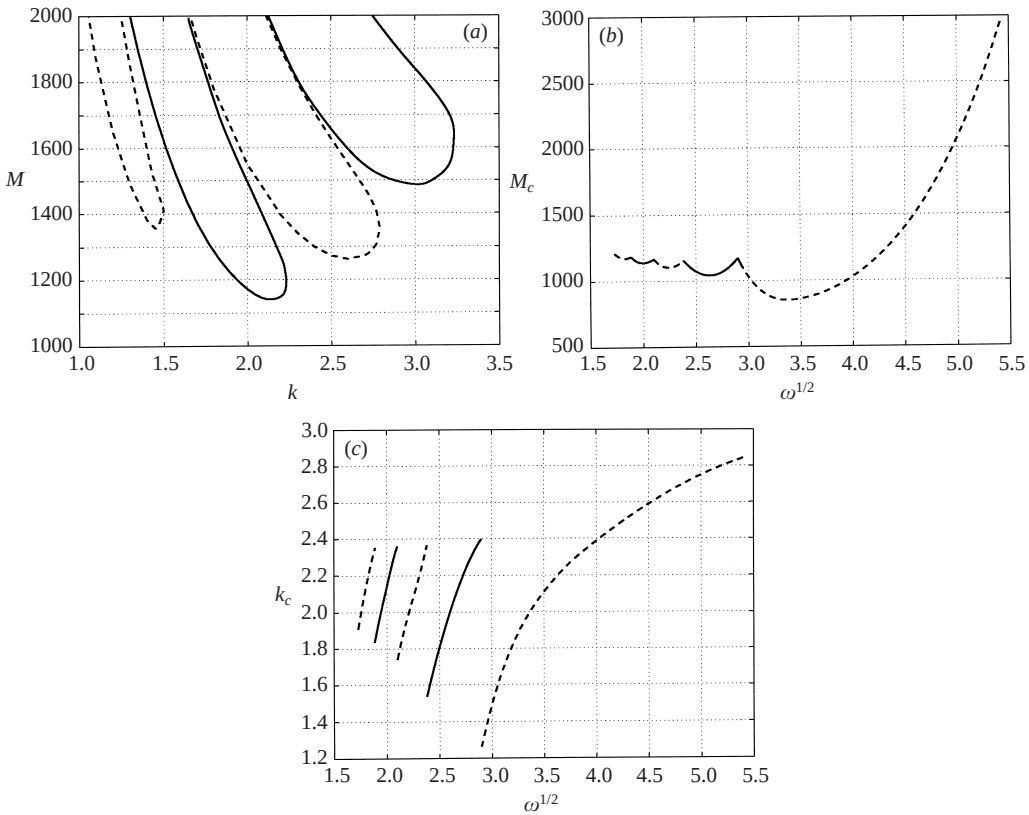

FIGURE 6. (*a*) Family of loop-shaped neutral curves for case (iii) showing a global minimum point which corresponds to the critical Marangoni number. (*b*) Critical curves showing M_c versus $\omega^{1/2}$ for a modulating basic state with prescribed temperature. (*c*) The corresponding critical wavenumber k_c.

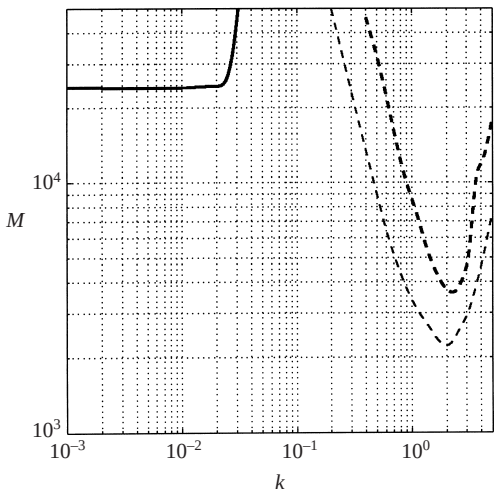

FIGURE 7. Neutral curve $M(k)$ of case (iv) showing the long-wavelength and finite-wavelength modes for $\omega^{1/2} = 3.5$ (thick lines: solid for S and dashed for H modes) and $\omega^{1/2} = 2$ (thin line).

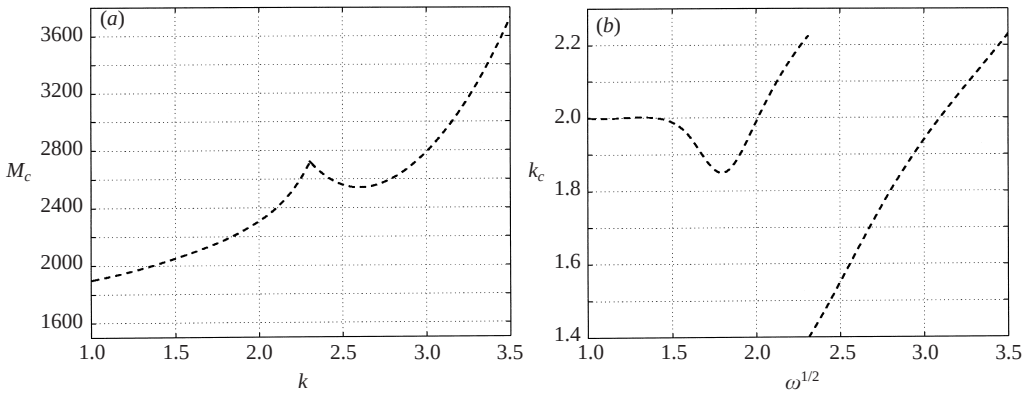

FIGURE 8. (*a*) Critical curves of case (iv) showing M_c versus $\omega^{1/2}$; for a modulating basic state with prescribed heat flux. (*b*) The corresponding critical wavenumber k_c.

increases monotonically as in figure 8(*b*). As ω decreases, the mode with the smaller scale becomes critical and the corresponding k_c eventually settles at approximately 2.0. Results for modulated Rayleigh–Bénard convection with zero mean and these boundary conditions are not available for comparison.

Qualitative similarity has been observed in the character of the stability boundaries between our problem and the MB convection subject to gravity modulation (Skarda 2001). For instance, the alternating synchronous and subharmonic unstable loop-shaped regions are displayed in figure 6 of Skarda. On the other hand, the stability boundaries reported in the gravity-modulated case appear to be significantly more complex than those we have obtained. From his figures 2 and 5, the occurrence of multiple humps and the isolated region of subharmonic instability have not been found in our case.

3.2. *Long-wavelength convection*

It is well known that long-wavelength modes can become the critical modes in unmodulated thermocapillary convection when the Galileo number (B/Cr) is small, such as in a microgravity environment, or when both of the thermal boundary conditions approach those appropriate for a fixed heat flux. The effect of vanishing gravity was discussed first by Scriven & Sternling (1964) and clarified by Smith (1966). In his figure 2, Pearson (1958) displayed neutral curves for the case of a fixed heat flux condition at the wall. As the Biot number of the free surface decreases, the values of both M_{c0} and k_c decrease until, at $Bi = 0$, the critical wavenumber becomes zero. In a footnote, Pearson correctly interpreted this limiting case as corresponding to a fixed heat flux at both surfaces. It is therefore appropriate to discuss how thermal modulation affects the onset of long-wavelength disturbances for these special boundary conditions. The $k \to 0$ limit allows significant simplification of the equations and boundary conditions and, by expanding the solution in terms of k, an explicit value for M_c can be obtained. When we extended this approach to include the effect of thermal modulation for $\omega \sim O(1)$ or greater, we found that for case (i) the modulation does not affect the critical Marangoni number which is therefore given by the unmodulated result. The question of whether long wavelength disturbances are preferred can be answered by comparing this value of M with the calculated value for the case of modulation when finite-wavelength disturbances are considered. For case (iii), we found neutral solutions only with k^2M remaining finite

as $k \to 0$, i.e. there is no instability at a finite value of M as $k \to 0$. However, we have already seen in figure 7 that solutions exist for low values of k at finite values of M for case (iv). We will therefore exclude the details of our analysis for cases (i) and (iii) in order to concentrate on cases (ii) and (iv). In order to limit further the analysis, we will consider only the condition of zero perturbation heat transfer at $z = 0$. Consistent with this boundary condition, we assume that the mean heat transfer is fixed at the free surface so $\Delta T^* = \bar{Q}^* d/K$.

For $k^2 \ll 1$ and with M finite, the free-surface shear-stress condition, equation (14), can be satisfied when $\Theta(z,t)$ and $N(t) \sim O(1)$ and $W(z,t) \sim O(k^2)$. By restricting our analysis to $\omega \sim O(1)$, the kinematic condition, equation (16), indicates that the lowest-order surface deflection, N_0, is constant. Since the coupling terms between the basic state and the perturbation typically occur in the terms $T_z(0,t)N_0$ and $T_{zz}(0,t)N_0$ at lowest order, a constant N_0 rules out a subharmonic solution in the long-wavelength limit. On the other hand, if a low-frequency limit $\omega \sim O(k^2)$ is to be considered, then N_0 is no longer necessarily time independent. A low-frequency analysis will require a separate study, and so here we restrict ω to be $O(1)$ or higher.

We seek a neutral stability condition for M, with

$$M = M_0 + O(k^2), \tag{20a}$$

where M_0 is a function of the physical and modulating parameters. Near $M = M_0$, we expect a modal growth rate γ to be of $O(k^2)$, i.e. $\gamma = \gamma_2 k^2$ where γ_2 is real. For long wavelength modes, W, Θ and N are expanded in terms of k^2, as

$$W(z,t) = k^2\{\bar{W}_2(z) + \hat{W}_2(z)\cos t + \check{W}_2(z)\sin t + \ldots\}\exp(k^2\gamma_2 t), \tag{20b}$$

$$\Theta(z,t) = \{\bar{\Theta}_0(z) + \hat{\Theta}_0(z)\cos t + \check{\Theta}_0(z)\sin t + \ldots\}\exp(k^2\gamma_2 t), \tag{20c}$$

$$N(t) = \{N_0 + k^2(\bar{N}_2 + \hat{N}_2\cos t + \check{N}_2\sin t) + \ldots\}\exp(k^2\gamma_2 t). \tag{20d}$$

With a more compact complex representation, we let $\tilde{\phi}_t(z) = \phi_{tc}(z) + \mathrm{i}\phi_{ts}(z)$, $\tilde{\phi}_f(z) = \phi_{fc}(z) + \mathrm{i}\phi_{fs}(z)$, $\tilde{\Theta}_0(z) = \hat{\Theta}_0(z) + \mathrm{i}\check{\Theta}_0(z)$, $\tilde{W}_2(z) = \hat{W}_2(z) + \mathrm{i}\check{W}_2(z)$, $\tilde{N}_2 = \hat{N}_2 + \mathrm{i}\check{N}_2$.

For the $O(1)$ balance of case (ii), we have

$$\bar{\Theta}_{0,zz}(z) = 0, \tag{21a}$$

subject to the upper and lower boundary conditions

$$\bar{\Theta}_{0,z}(0) = 0, \quad \bar{\Theta}_{0,z}(1) = 0. \tag{21b}$$

In equation (21b), we have used $T_{zz} = 0$ and N_0 is undetermined according to equation (15). Integrating equation (21a) and using the boundary conditions give

$$\bar{\Theta}_0(z) = b, \tag{22}$$

where b is constant. It can be determined as follows from the $O(k^2)$ heat balance by extending the analysis of Garcia-Ybarra, Castillo & Velarde (1987) to the case of modulation. From equation (9), we obtain

$$\bar{\Theta}_{2,zz}(z) - \overline{T_z(z,t)W_2(z,t)} - \bar{\Theta}_0(z) = 0. \tag{23}$$

The corresponding boundary conditions are

$$\overline{T_{zz}(0,t)N_2(t)} + \bar{\Theta}_{2,z}(0) = 0, \tag{24}$$

and

$$\bar{\Theta}_{2,z}(1) = 0. \tag{25}$$

Integrating equation (23) and making use of the boundary conditions (24) and (25), we have

$$b = \overline{T_{zz}(0,t)N_2(t)} - \int_0^1 (\overline{T_z(z,t)W_2(z,t)}\,\mathrm{d}z. \tag{26}$$

Using the expressions for the basic state, we write

$$b = \frac{\epsilon_F}{2}\left\{\phi''_{fc}(0)\hat{N}_2 + \phi''_{fs}(0)\check{N}_2 - \int_0^1 (\phi'_{fc}(z)\hat{W}_2(z) + \phi'_{fs}(z)\check{W}_2(z))\,\mathrm{d}z\right\} - \int_0^1 \bar{W}_2(z)\,\mathrm{d}z, \tag{27}$$

The last integral on the right-hand side involves the mean field that is governed by

$$\bar{W}_{2,zzzz}(z) = 0 \tag{28}$$

and satisfies the no-slip lower wall boundary conditions

$$\bar{W}_2(1) = \bar{W}_{2,z}(1) = 0. \tag{29}$$

It yields a solution of the form

$$\bar{W}_2(z) = c(z-1)^3 + d(z-1)^2. \tag{30}$$

The two constants c and d are determined from the two free-surface boundary conditions

$$-\bar{W}_{2,zzz}(0) = \frac{B}{Cr}N_0, \tag{31}$$

$$\bar{W}_{2,zz}(0) = M_0(N_0 + \bar{\Theta}_0(0)), \tag{32}$$

which give

$$c = -\frac{B}{6Cr}N_0, \quad d = 3c + \tfrac{1}{2}M_0\{N_0 + \bar{\Theta}_0(0)\}. \tag{33}$$

From equation (30), we obtain $\int_0^1 \bar{W}_2(z)\,\mathrm{d}z = -\frac{1}{4}c + \frac{1}{3}d$. The term in equation (27) involving the curly brackets has to be evaluated by solving independently for the fluctuating quantities. The development of the governing equations is included in Appendix A. It is clear from equation (32) that $\tilde{W}_2(z)$ is scaled by M_0. Moreover, both $\tilde{W}_2$ and $\tilde{\Theta}_0$ are scaled by $\epsilon_F N_0$. The deflection $\tilde{N}_2$ can be eliminated in terms of $\tilde{W}_2$ by use of the kinematic condition, yielding $\alpha^2\tilde{N}_2 = \tilde{W}_2$ when $\alpha = -\mathrm{i}2\omega$. Therefore, we introduce b_1, a constant independent of the parameters, and express the curly-bracket term as

$$\epsilon_F M_0 N_0 b_1 = \frac{1}{2}\left\{\phi''_{fc}(0)\hat{N}_2 + \phi''_{fs}(0)\check{N}_2 - \int_0^1 (\phi'_{fc}(z)\hat{W}_2(z) + \phi'_{fs}(z)\check{W}_2(z))\,\mathrm{d}z\right\}. \tag{34}$$

Therefore, equation (27) becomes

$$b = {\epsilon_F}^2 M_0 b_1 N_0 + \tfrac{1}{4}c - \tfrac{1}{3}d \tag{35}$$

where c and d are given by equation (33). From equation (30), $\bar{W}_2(0) = -c + d$, and with the kinematic condition $\gamma_2 N_0 = \bar{W}_2(0)$, we obtain

$$\gamma = \frac{k^2}{\frac{1}{3}M_0 + 2}\left\{\epsilon_F^2 M_0^2 b_1 + M_0\left(\frac{B}{72Cr} + 1\right) - \frac{2B}{3Cr}\right\}. \tag{36}$$

For the unmodulated situation $\epsilon_F = 0$, we recover

$$M_{0c} = \frac{48}{1 + 72Cr/B}, \tag{37}$$

in agreement with the result given by Garcia-Ybarra *et al.* (1987).

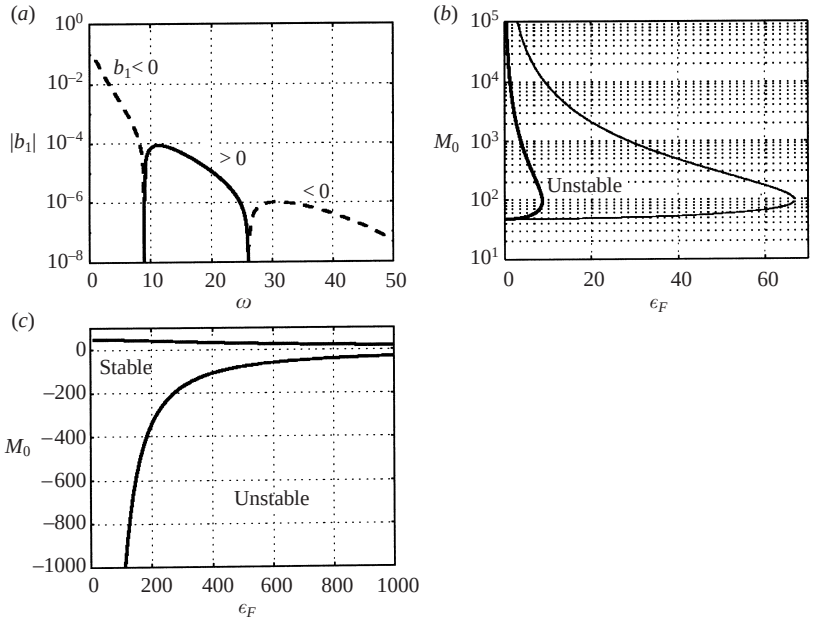

FIGURE 9. (*a*) The coefficient b_1 in a range of ω; (*b*) neutral curve M_0 in a range of ϵ_F, for $\omega = 1$ (thick) and $\omega = 6$ (thin), $Pr = 7$ and $B/Cr = 7.5 \times 10^4$ (case (ii)); (c) same for $\omega = 12$.

As will be shown, the stability behaviour with $\epsilon_F \neq 0$ is strongly influenced by the term involving b_1 in equation (36). The coefficient b_1 changes sign as ω varies and so it can be stabilizing or destabilizing, depending on whether b_1 is negative or positive. It also depends weakly on Pr. This term originates from the oscillating thermal field and gives a mean effect. In contrast to it, the second term in equation (36) (describing the Marangoni effect) is always destabilizing and the third term (describing the effects of gravity and surface tension) is always stabilizing; both are independent of ω and ϵ_F. In figure 9(*a*), we plot $|b_1|$ for $Pr = 7$ as a function of frequency. The dashed and solid portions of the curve indicate negative and positive b_1, respectively. Thus, the results show alternating stabilizing and destabilizing ranges of ω corresponding to the sign of the term $(\epsilon_F M_0)^2 b_1$.

We now explore in figures 9(*b*) and 9(*c*) the stability properties with M_0 over selected ranges of the modulating parameters ϵ_F and ω. Consider the earthbound condition $B/Cr = 7.5 \times 10^4$. In figure 9(*b*), we first show M_0 for $b_1 < 0$ for two values of ω, corresponding to $\omega = 1$ (thick line) and $\omega = 6$ (thin line). The region enclosed by the outer and inner branches of the neutral curve is unstable. As $\epsilon_F \to 0$, the inner branch has a finite value corresponding to the solution given by equation (37) but the outer branch diverges to infinity. Hence, moderate values of ϵ_F limit the range of instability. In both cases, when ϵ_F increases, the lower M_0 value increases mildly, indicating stabilization. When ϵ_F is sufficiently large, however, the two branches terminate at a nose. Beyond the nose, there is no long wavelength convection since the stabilizing term $(\epsilon_F M_0)^2 b_1$ is dominant. For these values of ω, the modulation is clearly stabilizing.

Now consider a higher frequency, $\omega = 12$, when $b_1 > 0$ and so the modulating term is destabilizing. The neutral curves are shown in figure 9(*c*). In a wide range of ϵ_F (from 0 to 10^3), no nose is found. The contribution of the destabilizing Marangoni

effect is augmented on the inner branch by the destabilizing effect of modulation. Therefore, M_0 continues to decrease as ϵ_F increases. However, now the outer branch corresponds to negative M_0. This situation suggests that an ordinarily stable situation (such as $\Delta T^* < 0$ or $\mathrm{d}\sigma/\mathrm{d}T^* > 0$) can become unstable if $(\epsilon_F M)^2$ is large enough. Note, however, that the values of ϵ_F required in figure 9(c) for instability with M_0 are indeed very large. For microgravity, the main effect is to reduce M_{0c} to zero as $B \to 0$. The qualitative effects of modulation do not change.

The cause of the flip-flop of sign of b_1 in figure 9(a), corresponding to $|M_0| = \infty$ at $b_1 = 0$, is revealed from the z-dependence of the basic state and the disturbance. The z-dependence of these functions is important for determining the integral on the right-hand side of equation (34). The surface terms, in contrast, make only a minor contribution to b_1. Consider the two frequencies $\omega = 2$ and $\omega = 12$, which are before and after the first singular point, at about $\omega \approx 9$. The z-dependence indicates that the integral of equation (34) is positive for $\omega = 2$ but negative for $\omega = 12$. The sign change is due to the sine terms $\phi'_{fs}(z)$ and $\breve{W}_2(z)$ rather than the cosine phase terms.

Now, we extend our discussion to the case with a zero-mean basic state, case (iv). With $\bar{T}^{(0)} = 0$, equation (33) gives

$$-M_0 b + 2d = 6c. \tag{38}$$

With a purely oscillating field, equation (26) becomes

$$b = M_0 N_0 b_1, \tag{39}$$

where $M_0 N_0 b_1$ is given by equation (34), since the integral of the $\bar{W}_2$ term vanishes. Note that the expression for b_1 is identical to that in case (ii) and that, owing to a rescaling, M_0 in case (iv) corresponds to $\epsilon_F M_0$ in case (ii).

Now, $\gamma = k^2 \bar{W}_2(0) = k^2(-c + d)$. Using equations (38) and (39), we have

$$\gamma = \frac{k^2}{2}\left\{ M_0^2 b_1 - \frac{2B}{3Cr} \right\}. \tag{40}$$

With the above rescaling in mind, it becomes apparent that equation (40) can be obtained directly from equation (36) of case (ii) by allowing $M_0 \to 0$ and $\epsilon_F \to \infty$ in equation (36), such that $\epsilon_F M_0$ remains finite. Unlike case (ii), in case (iv) the two branches of the neutral curve plotted against frequency are symmetric with respect to M_0, and are given by

$$M_0 = \pm F(\omega)\sqrt{\frac{2B}{3Cr}}, \quad F(\omega) = \frac{1}{\sqrt{b_1}}. \tag{41}$$

In figure 10(a), we plot $F(\omega)$ for a range of $\omega^{1/2}$ at $Pr = 7$. The region above each loop-shaped curve is unstable. To further explore the dependence on Pr, we consider the minimum point of the first loop of figure 10(a) and track this point by varying Pr. Figures 10(b) and 10(c) show, respectively, $F(\omega)$ and ω of this point for a range of Pr. The results show that M_0 diverges soon after Pr falls below one.

4. Concluding remarks

We have investigated the effects of thermal modulation upon a layer of fluid in two limits of the boundary conditions, namely, with a prescribed temperature or heat flux applied at the lower wall. The onset conditions of both finite- and long-wavelength MB convection have been obtained. In the results, the modulating frequency is

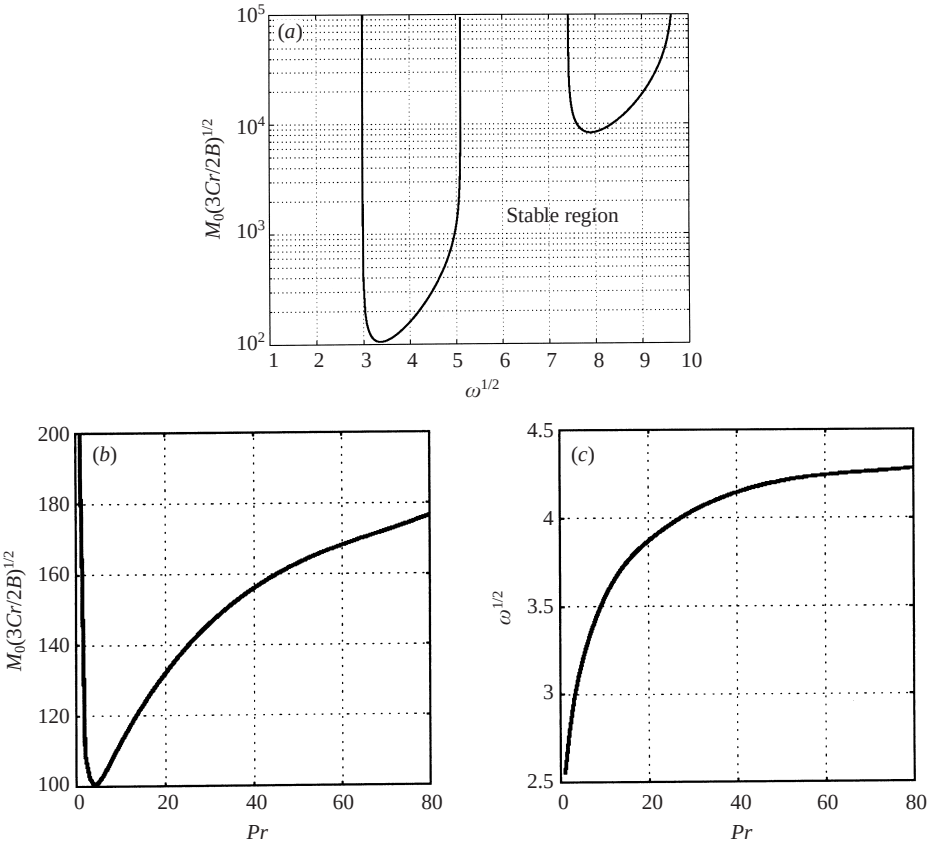

FIGURE 10. (*a*) First two branches of neutral curve of long wavelength convection at $Pr = 7$ (case (iv)). (*b*) Minimum of the first branch versus Pr; (*c*) the corresponding value of $\omega^{1/2}$ versus Pr.

assumed to be of $O(1)$ or larger. The layer of fluid is assumed to be sufficiently thin that the buoyancy force can be neglected.

For the finite-wavelength modes, the stability characteristics of cases (i) and (iii) are found to be similar to those of modulated RB convection reported earlier (see Yih & Li 1972; Swift & Hohenberg 1987). There are numerous loops of the critical curve in the ranges of ϵ_T and ω. With large ϵ_T, increasingly smaller loops appear as ω decreases toward zero. This type of behaviour was also found in the responses of an isothermal layer of viscous fluid with a free surface subject to gravity modulation (see Kumar 1996; Cerda & Tirapegui 1997). There is a major difference between modulated MB convection and RB convection that is worth noting. For large ω corresponding to the case of zero-mean basic state (case (iii)), there is no Stokes-layer type instability in MB convection according to our configuration. In our results, M_c and k_c do not vary according to the scalings of the thickness of the thermal Stokes layer. This is in contrast to modulated RB convection (Swift & Hohenberg 1987; Or & Kelly 1999).

Another dramatic difference is between the shapes of the critical curves which appear very different in the two cases of prescribed temperature and heat flux. For a wide range of modulating amplitude, significantly fewer loops appear in cases (ii) and (iv) than in cases (i) and (iii). In cases (ii) and (iv), only two loops of the

critical curve are found, both corresponding to subharmonic modes. We conclude that thermal modulation exerts significantly different effects in the two limits of prescribed temperature and heat flux.

The relative importance between the long-wavelength and finite-wavelength modes is controlled by the deformation parameter B/Cr. However, modulation also exerts some effect. For case (i), the modulation has no effect on the critical condition of long-wavelength convection, but it can exert a significant stabilizing influence on the finite-wavelength modes. Therefore, thermal modulation tends to make the long-wavelength mode more critical under certain circumstances. For case (ii), the deformable free surface tends to destabilize the long-wavelength mode moderately. The modulation possesses stabilizing or destabilizing effects in this limit, depending on frequency (in contrast, the modulation has a stabilizing effect on the onset of the finite-wavelength modes). For case (iii), there is no long-wavelength mode. For case (iv), M_c of the long-wavelength mode scales as $(B/Cr)^{1/2}$ but M_c of the finite-wavelength modes is about an order of magnitude larger than the value in case (ii). The long-wavelength mode can be more important than the finite-wavelength mode under reduced gravity.

This work has been supported by the NASA Microgravity Fluid Physics Program through Grant NAG3-1819.

Appendix A

Let us now consider the oscillating field in equations (20*b*) and (20*c*), which will be used to evaluate b in equation (27). At $O(1)$, $\tilde{\Theta}_0(z)$ is governed by

$$\tilde{\Theta}_{0,zz} - \alpha^2 \tilde{\Theta}_0 = 0, \tag{A 1a}$$

where $\alpha^2 = -\mathrm{i}2\omega$. The equation is subject to the boundary conditions

$$\tilde{\Theta}_{0,z}(1) = 0, \tag{A 1b}$$

$$\epsilon_F \tilde{\phi}_{t,zz}(0) N_0 + \tilde{\Theta}_{0,z}(0) = 0. \tag{A 1c}$$

The solution is given by

$$\tilde{\Theta}_0(z) = A\mathrm{e}^{\alpha z} + B\mathrm{e}^{-\alpha z}, \tag{A 1d}$$

where the complex constants A and B are given by

$$\begin{bmatrix} \alpha\mathrm{e}^{\alpha} & -\alpha\mathrm{e}^{-\alpha} \\ \alpha & -\alpha \end{bmatrix} \begin{bmatrix} A \\ B \end{bmatrix} = \begin{bmatrix} 0 \\ -\tilde{\phi}_{t,zz}(0)\epsilon_F N_0 \end{bmatrix}. \tag{A 1e}$$

Denoting $\tilde{N}_0 = \tilde{\phi}_{t,zz}(0)\epsilon_F N_0$, we obtain

$$A = \frac{\tilde{N}_0 \mathrm{e}^{-\alpha}}{2\alpha \sinh \alpha}, \quad B = \frac{\tilde{N}_0 \mathrm{e}^{\alpha}}{2\alpha \sinh \alpha}. \tag{A 2}$$

At $O(k^2)$, we have the boundary-value problem

$$\tilde{W}_{2,zzzz} - \beta^2 \tilde{W}_{2,zz} = 0, \tag{A 3a}$$

where $\beta^2 = Pr^{-1}\alpha^2$. The general solution of equation (A 3a) has the form

$$\tilde{W}_2(z) = Cz + D + E\mathrm{e}^{\beta z} + F\mathrm{e}^{-\beta z}, \tag{A 3b}$$

subject to the boundary conditions,

$$\tilde{W}_2(1) = \tilde{W}_{2,z}(1) = 0, \tag{A 3c}$$

$$-\tilde{W}_{2,zz}(0) = -M_0\{\epsilon_F \tilde{\phi}_{t,z}(0)N_0 + \tilde{\Theta}_0(0)\}, \tag{A 3d}$$

$$\beta^2 \tilde{W}_{2,z} - \tilde{W}_{2,zzz} = 0. \tag{A 3e}$$

Equation (16) determines $\tilde{N}_2$ once $\tilde{W}_2$ is known. From equation (A 3e), we conclude that $C = 0$. The other three coefficients are determined by

$$\begin{bmatrix} 1 & \mathrm{e}^{\beta} & \mathrm{e}^{-\beta} \\ 0 & \beta\mathrm{e}^{\beta} & -\beta\mathrm{e}^{-\beta} \\ 0 & -\beta^2 & -\beta^2 \end{bmatrix} \begin{bmatrix} D \\ E \\ F \end{bmatrix} = \begin{bmatrix} 0 \\ 0 \\ -M_0\{\epsilon_F \tilde{\phi}_{t,z}(0)N_0 + \tilde{\Theta}_0(0)\} \end{bmatrix}. \tag{A 3f}$$

Denoting $\hat{N}_0 = M_0(\epsilon_F \tilde{\phi}_{t,z}(0)N_0 + \tilde{\Theta}_0(0))$, equation (A 3f) can be solved to give

$$D = \frac{-\hat{N}_0}{\beta^2 \cosh\beta}, \quad E = \frac{\hat{N}_0 \mathrm{e}^{-\beta}}{2\beta^2 \cosh\beta}, \quad F = \frac{\hat{N}_0 \mathrm{e}^{\beta}}{2\beta^2 \cosh\beta}. \tag{A 4}$$

In the above, $\tilde{W}_2(z)$ can be determined once M_0, N_0 and $\tilde{\Theta}_0(0)$ are known, since the determinant of the matrix on the left-hand side does not vanish for β real and non-zero.

Appendix B

In laboratory experiments, a two-layer configuration occurs. For a single-layer model, it is important to justify that the basic-state temperature expressions, given by equations 7(a) and 7(b) for the purely oscillating temperature case (iii) and oscillating heat flux case (iv) at the lower wall, approximate well the liquid temperature for the two-layer model in the range of physical parameters used in this paper.

As in the time-independent problem, we can eliminate the governing equations of the gas by obtaining an interfacial condition of the form equation (5), where the Biot number is now an expression of the ratios of material properties of the two layers, the layer thicknesses and frequency. It turns out for the purely time-fluctuating case that the Biot number is complex. Below, it is shown that when the absolute value of the Biot number is small, then the one-layer model is a good approximation if Bi in equation (5) is chosen to be a small parameter.

For the purely conductive basic state, we have the heat diffusive equations $\tilde{T}_{g,t} = r_1 \tilde{T}_{g,zz}$ and $\tilde{T}_t = \tilde{T}_{zz}$ for the gas and liquid, respectively. The subscript g denotes the gas and $r_1 = \kappa_g/\kappa$.

For case (iii), assume that the boundary condition of the purely oscillating component temperature at the upper wall is

$$\tilde{T}_g(-\delta, t) = 0, \tag{B 1}$$

where $\delta = d_g/d$. We obtain the interfacial ($z = 0$) thermal condition

$$\tilde{T}_z(0, t) = Bi_c \tilde{T}(0, t), \tag{B 2}$$

where Bi_c is complex, given by

$$Bi_c = r_2 \sqrt{\frac{\mathrm{i}2\omega}{r_1}} \coth \sqrt{\frac{\mathrm{i}2\omega\delta^2}{r_1}}, \tag{B 3}$$

where $r_2 = K_g/K$.

For case (iv), assuming that the boundary condition of the purely oscillating component temperature for the upper wall is

$$(\tilde{T}_g)_z(-\delta, t) = 0, \tag{B 4}$$

with an interfacial temperature boundary condition given above from equation (B 2), we determine Bi_c to be

$$Bi_c = r_2\sqrt{\frac{\mathrm{i}2\omega}{r_1}}\tanh\sqrt{\frac{\mathrm{i}2\omega\delta^2}{r_1}}. \tag{B 5}$$

For air and silicone oil, $r_1 \gg 1$. If δ and ω are of $O(1)$, we obtain to $O((2\mathrm{i}\omega\delta^2/r_1)^{1/2})$,

$$Bi_c = \begin{cases} r_2/\delta = K_g d/K d_g & \text{for case (iii),} \\ r_2\mathrm{i}2\omega\delta/r_1 & \text{for case (iv).} \end{cases} \tag{B 6}$$

In case (iii), Bi_c is real, but in case (iv), Bi_c is purely imaginary. Furthermore, Bi_c is independent of ω for case (iii) as long as ω is $O(1)$, whereas Bi_c is a linear function of ω in case (iv).

We have performed the stability analysis based on the one-layer model with $Bi = 0.1$ in equations 7(a) and 7(b). Consider an example of a two-layer model with $\delta = 2$ and silicone oil for the liquid. This gives $r_1 = 2.4 \times 10^2$ and $r_2 = 0.2$. First, we have computed the basic temperature profile of the two-layer model and verified the expressions of Bi_c derived above. Secondly, we have compared the temperature profiles in the range of ω from 0.8 to 10, for both cases (iii) and (iv). For case (iii), $\mathrm{Re}\{Bi_c\} \sim 0.1$ and $\mathrm{Im}\{Bi_c\}$ varies from 10^{-2} to 10^{-3} in the frequency range. For case (iv), $\mathrm{Re}\{Bi_c\} \sim \mathrm{Im}\{Bi_c\}$, both are $O(10^{-2})$ in the frequency range used. Therefore, $|Bi_c| \ll 1$. The difference in the basic temperature is so small that we cannot distinguish between the two profiles. This example suggests that the one-layer approximation is good for the two-layer configuration as far as the basic state is concerned.

REFERENCES

Cerda, E. & Tirapegui, E. 1997 Faraday's instability for viscous fluids. *Phys. Rev. Lett.* **78**, 859–862.

Davis, S. H. 1976 The stability of time-periodic flows. *Annu. Rev. Fluid Mech.* **8**, 57–74.

Donnelly, R. J. 1990 Externally modulated hydrodynamic systems. In *Nonlinear Evolution of Spatial-temporal Structures in Dissipative Continuous Systems* (ed. F. H. Busse & L. Kramer), pp. 31–43. Plenum Press, NY.

Garcia-Ybarra, P. L., Castillo, J. L. & Velarde, M. G. 1987 Bénard–Marangoni convection with a deformable interface and poorly conducting boundaries. *Phys. Fluids* **30**, 2655–2661.

Gershuni, G. Z., Nepomnyashchy, A. A. & Velarde, M. G. 1992 On dynamic excitation of Marangoni instability. *Phys. Fluids* **4**, 2394–2398.

Golovin, A. A., Nepomnyashchy, A. A. & Pismen, L. M. 1995 Pattern formation in large-scale Marangoni convection with deformable interface. *Physica* D **81**, 117–147.

Kamotani, Y. 1997 Surface tension driven convection in microgravity. *Adv. Astro. Sci.* **96**, 487–499.

Kelly, R. E. & Or, A. C. 1998 Influence of temperature modulation upon the onset of thermo-capillary convection. *AIAA Paper* 98-0652.

Kumar, K. 1996 Linear theory of Faraday instability in viscous liquids. *Proc. R. Soc. Lond.* A **452**, 1113–1126.

Niemela, J. J. & Donnelly, R. J. 1986 Instability of a thermal Stokes layer. *Phy. Rev. Lett.* **57**, 583.

Or, A. C. 1997 Finite wavelength instability in a horizontal liquid layer on an oscillating plane. *J. Fluid Mech.* **335**, 213–232.

Or, A. C. 2001 Onset condition of modulated Rayleigh–Bénard convection at low frequency. *Phys. Rev.* E **64**, 1–3.

Or, A. C. & Kelly, R. E. 1995 Onset of Marangoni convection in a layer of fluid modulated by a weak nonplanar oscillatory shear. *Intl J. Heat Mass Transfer* **38**, 2269–2279.

Or, A. C. & Kelly, R. E. 1998 Thermocapillary and oscillatory-shear instabilities in a layer of liquid with a deformable surface. *J. Fluid Mech.* **360**, 21–39.

Or, A. C. & Kelly, R. E. 1999 Time-modulated convection with zero-mean temperature gradient. *Phys. Rev.* E **60**, 1741–1747.

Pearson, J. R. A. 1958 On convection cells induced by surface tension. *J. Fluid Mech.* **4**, 4890–500.

Pérez-García, C., Echebarria, B. & Bestehorn, M. 1998 Thermal properties in surface-tension-driven convection. *Phy. Rev.* E **57**, 475–481.

Regnier, V. C., Dauby, P. C. & Lebon, G. 2000 Linear and nonlinear Rayleigh–Bénard–Marangoni instabilities with surface deformations. *Phys. Fluids* **12**, 2787–2799.

Scriven, L. E. & Sternling, C. V. 1964 On cellular convection driven surface tension gradients: effects of mean surface tension and surface viscosity. *J. Fluid Mech.* **19**, 321–340.

Skarda, J. R. E. 2001 Instability of a gravity-modulated fluid layer with surface tension variation. *J. Fluid Mech.* **434**, 243–271.

Smith, K. A. 1966 On convection instability induced by surface tension. *J. Fluid Mech.* **24**, 401–414.

Swift, J. B. & Hohenberg, P. C. 1987 Modulated convection at high frequencies and large modulation amplitudes. *Phy. Rev.* A **36**, 4870.

Yih, C. S. & Li, C. H. 1972 Instability of unsteady flows or configurations. Part 2. Convective instability. *J. Fluid Mech.* **54**, 143–152.